International Journal of Engineering and Technology Innovation, vol. 16, no. 4, 2026, pp. 526-536

Machine Learning-Based Fault Diagnosis for Rooftop Photovoltaic Systems

Mi Sa Nguyen Thi, Xuan-Duy Do, Dinh-Nguyen Tran, Dinh-Nhon Truong, Van-Phuong Ta*

Faculty of Electrical and Electronics Engineering, Ho Chi Minh City University of Technology and Engineering, Vietnam

Received 09 June 2026; revised 17 July 2026; accepted 21 July 2026

DOI: https://doi.org/10.46604/ijeti.2026.16514

Abstract

This study aims to develop a deep learning framework for intelligent fault detection, classification, and multi-level localization in rooftop photovoltaic (PV) systems. The proposed approach uses a hybrid CNN–LSTM architecture that combines a one-dimensional convolutional neural network (1D-CNN) to identify local spatial patterns with long short-term memory (LSTM) units to capture long-term temporal dependencies in time-series data. The framework was evaluated on a multivariate dataset collected from a grid-connected experimental rooftop PV prototype under various fault scenarios. Experimental results demonstrate that the hybrid model significantly outperforms standalone 1D-CNN and LSTM architectures across all evaluation criteria. Specifically, the proposed framework achieved classification accuracies of 99.96% for fault type identification, 98.76% for string-level fault localization, and 99.21% for module-level fault localization. These findings highlight the effectiveness and robustness of the hybrid framework for real-time monitoring and reliable fault diagnosis in photovoltaic installations.

Keywords: rooftop photovoltaic, fault diagnosis, hybrid CNN–LSTM, data-driven, deep learning

1. Introduction

The escalating global demand for clean and sustainable energy has significantly accelerated the adoption of rooftop photovoltaic systems (RPS) as an important component of modern power systems [1]. By enabling decentralized electricity production, RPS effectively reduce reliance on fossil fuels while contributing substantially to the mitigation of greenhouse gas emissions [2]. However, these systems are frequently exposed to highly dynamic and harsh environmental conditions, where factors such as intense solar irradiance, temperature fluctuations, dust accumulation, and extreme weather events can severely impact performance and operational lifespan. Such adverse conditions often lead to various fault types, including string-to-string (STS), string-to-ground (STG), and open-circuit (OC) faults [3-5]. If these anomalies are not detected and addressed promptly, they can result in significant power losses, accelerated equipment deterioration, and serious safety hazards [6].

To ensure the reliability and efficiency of PV systems, numerous diagnostic techniques have been explored. Conventional fault diagnosis methods are primarily based on analytical models, threshold-based techniques, or hardware-intensive monitoring. While these provide a baseline for system health, they often exhibit limitations such as low sensitivity to incipient faults and a heavy dependence on accurate mathematical models [7]. To overcome these limitations, signal-processing-based techniques have been introduced to extract fault-related characteristics from electrical signals through time–frequency analysis, wavelet transforms, and current–voltage (I–V) curve interpretation [8].

In recent years, data-driven approaches based on machine learning (ML) and deep learning (DL) have gained considerable attention due to their ability to model complex nonlinear relationships directly from operational data. Advanced architectures, particularly one-dimensional convolutional neural networks (1D-CNNs) and long short-term memory (LSTM) networks, have

* Corresponding author. E-mail address: phuongtv@hcmute.edu.vn

demonstrated outstanding performance in automatically learning patterns from time-series data [9]. Specifically, 1D-CNNs are effective for extracting local spatial and temporal features, while LSTM networks excel at modeling sequential data and preserving temporal information through gated memory mechanisms [10].

Despite these advancements, several research gaps persist. Most existing studies focus primarily on fault detection and classification, while fault localization at the module and string levels remains insufficiently investigated. Furthermore, many current approaches rely on high-dimensional datasets or additional sensing infrastructure, which increases implementation complexity and operational costs [11]. Regarding architecture, 1D-CNN models have limited capability for capturing the long-term temporal dependencies inherent in PV dynamics. Conversely, while LSTM networks are advantageous for historical context, they are often less effective in extracting localized discriminative features. Additionally, many studies have been conducted under controlled laboratory conditions rather than in real-world rooftop PV environments, which limits their practical applicability [12].

This study proposes a hybrid CNN–LSTM framework that integrates the complementary strengths of both architectures for multi-level fault diagnosis. By combining the spatial feature extraction of 1D-CNNs with the sequential learning capabilities of LSTM networks, the proposed model aims to achieve simultaneous fault type classification, string-level localization, and module-level identification [13]. This study focuses on using a minimal set of commonly available signals, including string currents, string voltages, and ambient temperature, to provide a robust, scalable, and highly accurate solution for real-time monitoring in actual photovoltaic installations. This integrated approach is expected to provide a more comprehensive spatio-temporal feature representation than standalone models, thereby improving reliable performance under real-world uncertainties.

2. Proposed Solution

This study proposes a comprehensive deep learning framework for multi-level fault detection and diagnosis in rooftop photovoltaic (PV) systems. The proposed framework is designed to simultaneously achieve three key diagnostic objectives: fault type classification (including string-to-string (STS), string-to-ground (STG), and open-circuit (OC) faults), string-level fault localization, and module-level fault localization. To effectively model the complex spatio-temporal behaviour of rooftop PV systems, a hybrid CNN–LSTM architecture is introduced. This integrated approach combines the feature extraction capability of 1D-CNNs with the sequential learning strength of LSTM networks, thereby enabling robust and efficient feature learning from multivariate time-series data.

The hybrid model begins with a 1D-CNN architecture, which is employed as the primary framework for fault classification due to its effectiveness in extracting local temporal features from time-series data. The 1D-CNN architecture is described as follows:

Given a multivariate input signal $x(t, j)$, the convolution output of the r^{th} channel at position t is defined as:

$$y_r(t) = f\left(\sum_{j=1}^{K}\sum_{i=0}^{L-1} x_j(st+i)w_{r,j}(i) + b_r\right), \qquad r = 1,2,...,R \tag{1}$$

where j denotes input feature index (channel index), $j = 1,2,\dots,K$; $x_j(\cdot)$ is the input signal of the j^{th} feature; $y_r(t)$ is the output of the r^{th} filter at position t; K is the number of input features; L is the kernel size along the temporal dimension;R is the number of filters; $w_{ij}(i)$ denotes i^{th} kernel weight connecting j input feature to filter output$r$; b_r is the bias term; s is the stride of convolution operation; t is the temporal index; and $f(\cdot)$ is the activation function introducing non-linearity. The overall architecture of the proposed hybrid CNN–LSTM framework is illustrated in Fig. 1.

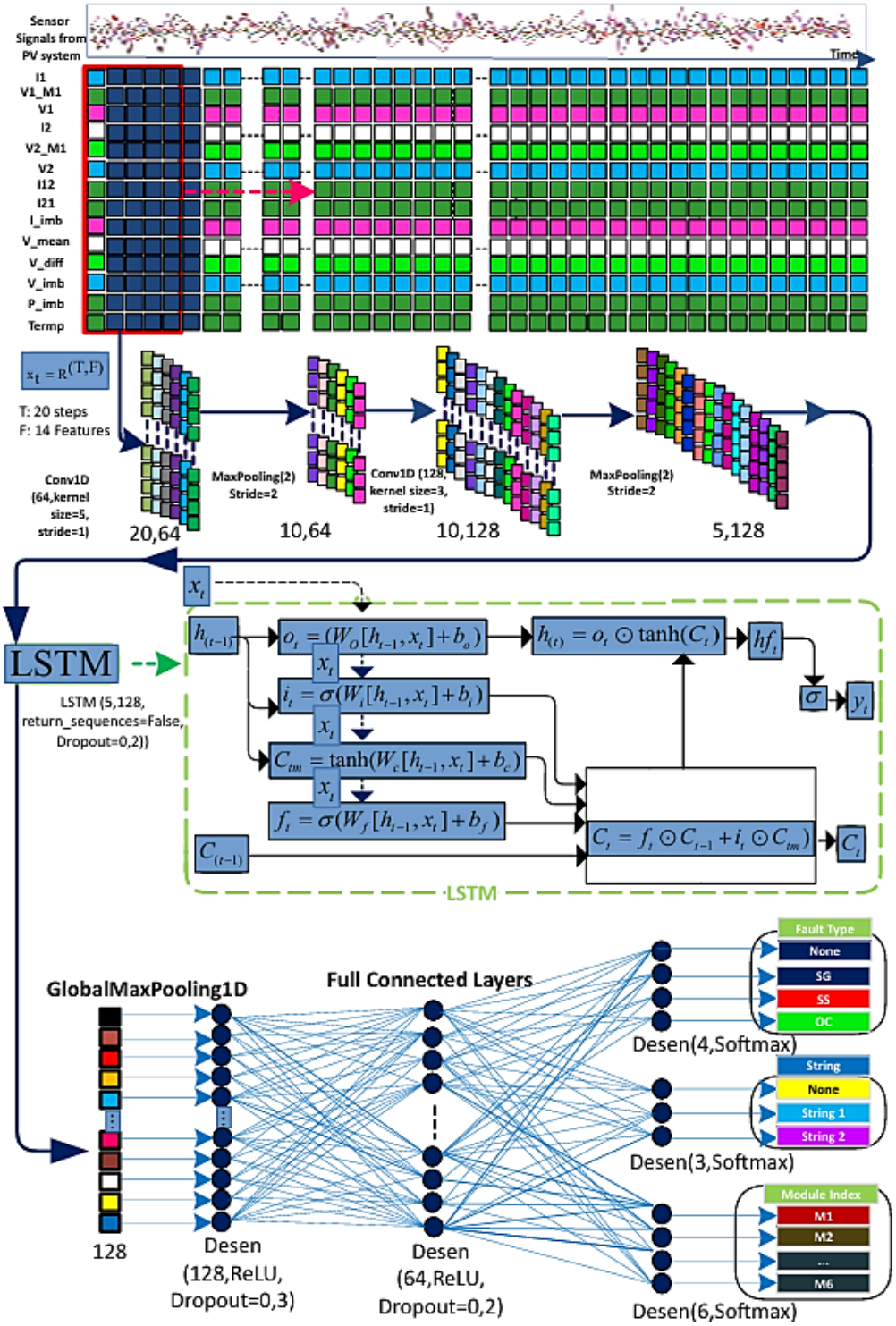


Fig. 1 Hybrid CNN-LSTM architecture for rooftop photovoltaic systems

In convolutional neural networks (CNNs), activation functions play a fundamental role in introducing non-linearity into the model, thereby enabling the extraction of complex temporal patterns embedded in time-series data. Various activation functions have been proposed, including Leaky ReLU, ELU, and GELU. Nevertheless, the rectified linear unit (ReLU) remains the most widely adopted activation function in time-series analysis [14]. Its popularity can largely be attributed to its computational efficiency, structural simplicity, and consistently strong empirical performance across diverse deep learning applications. The ReLU function is mathematically defined as follows:

$$f(z) = \max(0, z) \tag{2}$$

where z denotes the input to the activation function.

Following the convolution and activation stages, a pooling layer is employed to reduce the temporal dimensionality of the extracted feature maps while retaining the most informative characteristics [15]. Among the various pooling techniques, max pooling is the most widely adopted due to its effectiveness in capturing salient local features. Specifically, max pooling selects the maximum value within each pooling window, thereby preserving significant activations and fault-related patterns while suppressing irrelevant noise [16]. This process not only reduces computational complexity and improves generalization capability, but also enhances robustness against minor temporal variations in feature patterns, making it particularly suitable for time-series fault detection tasks. The max pooling operation is mathematically expressed as:

$$p_r(t_p) = \max_{i=0}^{M-1} y_r(t_p s + i) \tag{3}$$

where $p_r(t_p)$ denotes pooled output of the r^{th} feature map at pooled outputtemporal index t_p, M denotes pooling window size, s is the stride of the pooling operation, i is the index within the pooling window, y_r is the output of the r^{th} filter at position *t*.

To effectively capture temporal dependencies and sequential dynamics in time-series data, an LSTM network is employed. Unlike 1D-CNNs, which primarily extract local temporal patterns within fixed receptive fields, LSTM networks are specifically designed to model long-term dependencies across time steps through gated recurrent mechanisms. This capability makes LSTM particularly advantageous for tasks where historical context and temporal continuity play a critical role [17].

At each time step *t*, the LSTM cell maintains and updates both a hidden state h_t and a cell state C_t, enabling the selective retention and propagation of relevant information over long temporal sequences [18].

The cell state functions as a persistent memory mechanism that enables the retention and propagation of long-term dependencies across time steps, while the hidden state represents the current output and encodes short-term contextual information of the network. The interaction between these states is regulated by a set of gating mechanisms—including input, forget, and output gates—which regulate information flow and mitigate issues such as vanishing gradients. These operations are formally described through nonlinear gating functions and state update equations, as follows:

$$f_t = \sigma(W_f[h_{t-1}, x_t] + b_f) \tag{4}$$

$$i_t = \sigma(W_i[h_{t-1}, x_t] + b_i) \tag{5}$$

$$C_{tm} = \tanh(W_c[h_{t-1}, x_t] + b_c) \tag{6}$$

$$C_t = f_t \odot C_{t-1} + i_t C_{tm}) \tag{7}$$

$$o_t = (W_O[h_{t-1}, x_t] + b_o) \tag{8}$$

$$h_t = o_t \odot \tanh(C_t) \tag{9}$$

where x_t denotes the input at time step *t*; $h_{t-1}$and C_{t-1} represent the hidden and cell states from the previous time step; W_f, W_i, W_c, W_o and b_f, b_i, b_c, b_o are learnable weight matrices and bias terms; $\sigma(\cdot)$ is the sigmoid activation function; and $\odot$ denotes element-wise multiplication.

The forget gate f_t controls the retention of past information, the input gate i_t determines the amount of new information to be stored, and the output gate o_t regulates the information propagated to the next layer.

Through these mechanisms, the LSTM effectively captures both short-term variations and long-term dependencies, making it highly suitable for modeling complex temporal patterns in PV time-series data. The processing of temporal information within the LSTM unit is illustrated in Fig. 2.

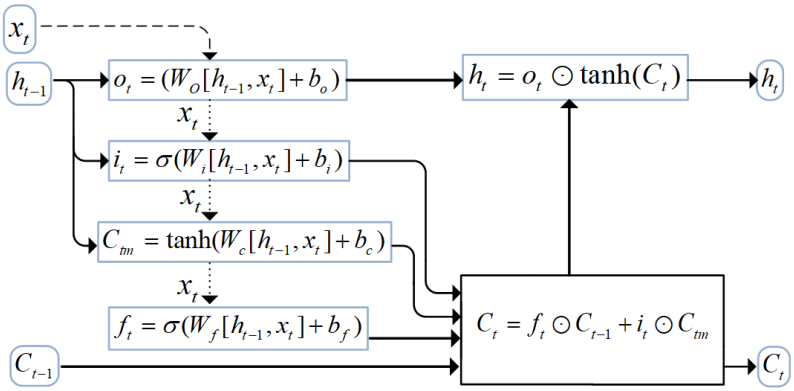


Fig. 2 The processing of temporal information within the LSTM

3. Experiment Setup

3.1 Experimental platform of the rooftop photovoltaic system

The experimental platform consists of a 5-kWp grid-connected (on-grid) rooftop photovoltaic (PV) system composed of two parallel strings, each comprising six series-connected modules, interfaced with a three-phase grid through a KacoBlueplanet 10.0 TL3 inverter. The overall configuration of the experimental platform is illustrated in Fig. 3.

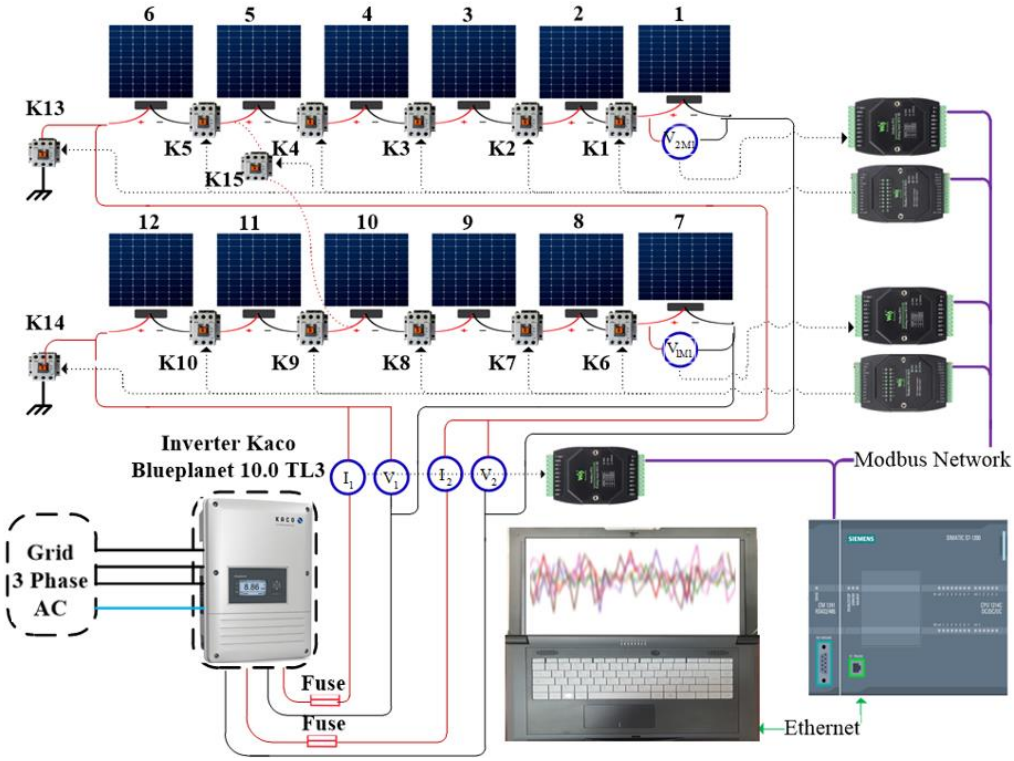


Fig. 3 Experimental platform of the research rooftop photovoltaic system

The architecture integrates a reconfigurable contactor-based switching network, multi-level sensing, and a real-time data acquisition system, enabling both normal operation and controlled fault injection for data-driven analysis. The PV strings are connected in parallel at the DC bus, reflecting a typical rooftop installation and ensuring realistic operational conditions.

A flexible reconfiguration network is implemented using contactors, where K1–K5 and K6–K10 control module-level interconnections in String 1 and String 2, respectively, allowing the emulation of open-circuit faults, mismatch conditions, and partial shading scenarios. At the string level, contactors K11 and K12 enable grounding and isolation of each string to simulate insulation and ground faults, while K13 provides cross-string interconnection for generating complex fault conditions such as leakage currents and inter-string disturbances.

The system is equipped with a hierarchical sensing structure, including string-level measurements of voltage (V_1,V_2) and current (I_1, I_2) to capture global behavior, as well as module-level measurements (V_{1M1} and V_{2M1}) corresponding to the first module in each string, enabling localized fault detection and diagnosis. Additionally, a temperature transmitter is incorporated to account for environmental influences on PV performance. The specifications of the PV modules and inverter used in the experimental setup are presented in Table 1.

Table 1 Specifications of the inverter and solar panel

Inverter		Solar Panel	
Manufacturer	KACO new energy	Manufacturer	Sharp corporation
Model	Blueplanet 10.0 TL3 M2	Photovoltaic module model	NU-JD440
Inverter type	Three-phase grid-connected	Maximum power (Pmax)	440 Wp
Rated apparent power	10 kVA	Open-circuit voltage	49.77 V (±10%)
Maximum DC input voltage	1000 V	Short-circuit current	11.49 A (±10%)
MPPT voltage range	470–800 V	Voltage at maximum power (Vmpp)	41.20 V
DC operating voltage range	200–950 V	Current at maximum power (Impp)	10.68 A
Nominal AC voltage	230 V / 400 V (3/N/PE)	Maximum system voltage	1500 V
Maximum continuous AC output current	3 × 15.5 A	Maximum over-current protection	20 A
Grid frequency	45–65 Hz	-	-

All sensor data are acquired via distributed remote stations and transmitted through a Modbus communication network to a Siemens SIMATIC S7-1200 programmable logic controller (PLC), which interfaces with a supervisory computer via Ethernet for real-time monitoring, storage, and analysis.

3.2 Prototype implementation of the rooftop photovoltaic system

To validate the proposed fault diagnosis framework under realistic operating conditions, a full-scale experimental prototype was developed, comprising both a rooftop PV installation and an indoor control cabinet. The prototype represents a complete cyber-physical PV system integrating power generation, monitoring, control, and fault injection capabilities.

The rooftop PV system consists of multiple photovoltaic modules mounted on an inclined roof structure, replicating typical real-world installation conditions. The panels are arranged in string configurations and exposed to natural environmental variations, including solar irradiance and temperature fluctuations. This setup ensures that the acquired data reflects realistic operating conditions, including dynamic changes in electrical output due to environmental factors.

The generated DC power from the rooftop PV array is routed to an indoor control cabinet, which serves as the central hub for power conversion, measurement, control, and data acquisition. The PLC communicates with distributed measurement modules via a Modbus network, enabling real-time acquisition of electrical signals, including string currents, string voltages, module-level voltages, and environmental temperature.

To enable systematic fault simulation, a contactor-based switching network is implemented inside the cabinet. This network corresponds to the defined contactors (K1–K13) and allows controlled emulation of various fault scenarios, including open-circuit faults, ground faults, and cross-string faults. The modular arrangement of contactors facilitates flexible reconfiguration of the PV strings and supports repeatable experimental conditions.

3.3 Dataset construction

To establish a comprehensive dataset for fault diagnosis, a total of 14 input features were extracted from the experimental rooftop PV system, combining both directly measured signals and derived features to capture the electrical behavior of the system under various operating conditions. Specifically, seven primary features were acquired directly from the experimental setup and were subsequently normalized to a range of [0, 1] to ensure numerical stability and improve model convergence.

These features include the string currents $I_1$and I_2, the string voltages V_1 and V_2, the module-level voltages of the first module in each string V_{1M1} and V_{2M1}, and the environment temperature. The normalized variables are denoted as I_{1_norm}, I_{1_norm}, V_{1_norm}, V_{2_norm}, V_{1M1_norm}, V_{2M1_norm}, and $temp_{norm}$.

To enhance the discriminative capability of the dataset, seven additional features were derived from the primary measurements to characterize current distribution, voltage imbalance, and power asymmetry between the two strings. These additional features are defined as:

$$I_{12}_norm = \frac{I_1_norm}{I_1_norm + I_2_norm + \varepsilon} \tag{10}$$

$$I_{21}_norm = \frac{I_2_norm}{I_1_norm + I_2_norm + \varepsilon} \tag{11}$$

$$I_{imb}_norm = \frac{I_1_norm - I_2_norm}{I_1_norm + I_2_norm + \varepsilon} \tag{12}$$

$$P_{imb}_norm = \frac{P_1_norm - P_2_norm}{P_1_norm + P_2_norm + \varepsilon} \tag{13}$$

$$V_{mean}_norm = \frac{V_1_norm + V_2_norm}{2} \tag{14}$$

$$V_{diff}_norm = V_1_norm - V_2_norm \tag{15}$$

$$V_{imb}_norm = \frac{V_1_norm - V_2_norm}{V_1_norm + V_2_norm} \tag{16}$$

where $\varepsilon = 10^{-6}$ is a small constant introduced to avoid division by zero.

These derived features are specifically designed to capture inter-string inconsistencies and suppress common-mode variations, thereby improving fault sensitivity.

The dataset comprises 35,508 time-series samples, each represented by 14 input features, and was randomly divided into training (70%), validation (15%), and testing (15%) subsets. This resulted in 24,855 samples for model training, 5,326 samples for validation and hyperparameter tuning, and 5,327 samples for independent performance evaluation. The input sequences and the three corresponding output labels—fault type, faulty string, and faulty module—were partitioned simultaneously to preserve the correspondence between each input sample and its associated multi-output targets.

The proposed hybrid CNN–LSTM model was trained using TensorFlow in the Google Colab environment with an NVIDIA T4 GPU. The trained model was subsequently deployed for real-time fault diagnosis on a standard PC equipped with an Intel(R) Core(TM) i5-14500 processor (2.60 GHz) and 16 GB RAM. The ability to perform inference without GPU acceleration demonstrates the suitability of the proposed framework for practical real-time PV monitoring applications.

4. Results and Discussion

The dataset was constructed by considering 31 unique combinations of fault type, fault location, and module index, encompassing normal operation, string-to-earth faults, string-to-string faults, and open-circuit conditions. For each combination, over 1,146 samples were collected, resulting in a total of 35,508 samples. Each sample consists of 14 input features, yielding a total of 497,112 data points for training and evaluation. The resulting multivariate time-series dataset was utilized to train and validate the proposed deep learning framework based on 1D-CNN and LSTM networks, enabling accurate fault classification and localization in the PV system.

The performance of the proposed fault diagnosis framework was evaluated using four standard classification metrics, namely accuracy, precision, recall, and F1-score. The evaluation was conducted at three levels: fault type classification, string-level localization, and module-level localization. A comparative analysis of the fault type classification performance of the 1D-CNN, LSTM, and hybrid CNN-LSTM models is presented in Table 2.

Table 2 Fault type classification performance

Model	Accuracy (%)	Precision (%)	Recall (%)	F1-score (%)
1D-CNN	99.64	99.64	99.64	99.63
LSTM	99.91	99.91	99.91	99.91
Hybrid CNN-LSTM	99.96	99.96	99.96	99.96

As shown in Table 2, all three models achieved excellent performance in fault type classification. However, the Hybrid CNN-LSTM model demonstrated the best overall results, consistently outperforming the 1D-CNN and LSTM models across all evaluation metrics. Specifically, the Hybrid CNN-LSTM attained an accuracy, precision, recall, and F1-score of 99.96%, surpassing the LSTM model's 99.91% and the 1D-CNN model's 99.64% accuracy and precision values. These findings indicate that integrating CNN and LSTM architectures enables the hybrid model to capture both spatial features and temporal dependencies more effectively, thereby enhancing classification performance and robustness in photovoltaic fault diagnosis.

Table 3 presents the performance results for string-level fault localization. Similar to the fault classification task, the Hybrid CNN-LSTM model achieved the highest performance across all evaluation metrics, outperforming both the standalone 1D-CNN and LSTM architectures. In particular, the Hybrid CNN-LSTM attained an accuracy, precision, recall, and F1-score of 98.76%, exceeding the LSTM model's 98.65% and significantly surpassing the 1D-CNN model's results of approximately 95.04–95.06%. These findings demonstrate that the hybrid architecture is more effective at capturing both local spatial patterns and long-term temporal dependencies within PV string data. Consequently, the proposed Hybrid CNN-LSTM model provides more accurate and reliable string-level fault localization, making it highly suitable for real-time photovoltaic monitoring and diagnostic applications.

Table 3 String-level localization performance

Model	Accuracy (%)	Precision (%)	Recall (%)	F1-score (%)
1D-CNN	95.04	95.06	95.04	95.04
LSTM	98.65	98.65	98.65	98.65
Hybrid CNN-LSTM	98.76	98.76	98.76	98.76

Module-level fault localization represents the most challenging diagnostic task, as it requires the identification of subtle variations within individual strings. As presented in Table 4, the hybrid CNN–LSTM architecture consistently demonstrates superior performance. Specifically, the proposed hybrid model achieves the highest accuracy, recall, and F1-score of 99.21%, along with a precision of 99.22%, outperforming the LSTM model, which achieves 98.61% across all evaluation metrics, and the 1D-CNN model, which records 96.32% accuracy, recall, and F1-score, with a precision of 96.35%.

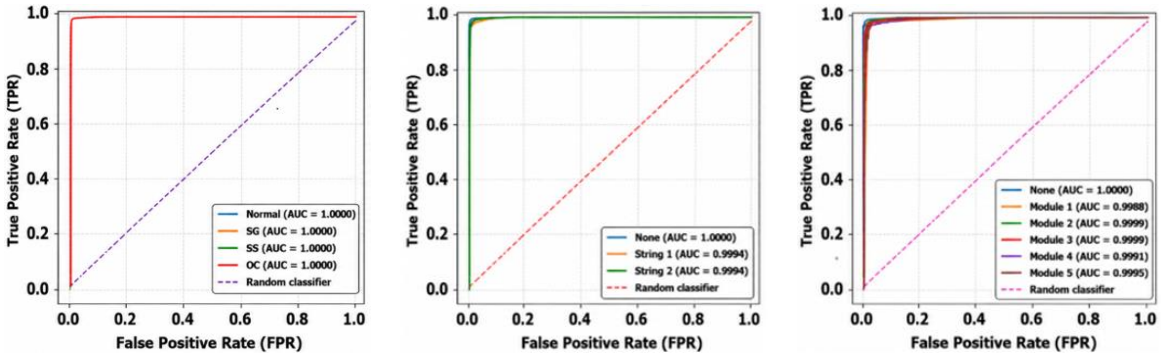
Table 4 Module-level localization performance

Model	Accuracy (%)	Precision (%)	Recall (%)	F1-score (%)
1D-CNN	96.32	96.35	96.32	96.32
LSTM	98.61	98.61	98.61	98.61
Hybrid CNN-LSTM	99.21	99.22	99.21	99.21

The performance gap becomes more evident at the module level due to the increased complexity and finer granularity of the classification task. The superior performance of the hybrid CNN–LSTM model suggests that the effective integration of local feature extraction and long-term temporal dependency modelling is essential for accurate module-level fault diagnosis.

Compared with recently published fault diagnosis methods, which reported accuracies ranging from 81.73% to 99% [13], the proposed hybrid model achieved better performance in terms of accuracy, precision, recall, and F1-score.

In addition to the fault type classification results, the performance of the proposed hybrid CNN–LSTM model was further evaluated for string-level and module-level fault localization using receiver operating characteristic (ROC) curves and the corresponding area under the curve (AUC) values. As illustrated in Fig. 4, the ROC curves for all three classification tasks are concentrated near the upper-left corner, demonstrating excellent discriminative capability. Furthermore, the AUC values approach 1.0 for all classes, confirming the high accuracy, robustness, and reliability of the proposed model in fault classification and localization.



(a) Fault type (b) String localization (c) Module localization

Fig. 4 The ROC curves and AUC of the hybrid CNN-LSTM model

The experimental results highlight the significant influence of model architecture on the performance of photovoltaic (PV) fault diagnosis. While the 1D-CNN effectively captures local temporal features, the LSTM consistently outperforms it across all evaluation metrics, emphasizing the importance of modeling temporal dependencies in PV time-series data. This advantage becomes increasingly evident as task complexity grows, particularly in string-level and module-level fault localization.

From a physical perspective, PV faults such as open-circuit and ground faults introduce time-varying fluctuations in current and voltage signals. The LSTM's capability to retain sequential information enables more effective learning of these evolving patterns, whereas the 1D-CNN is limited to short-range feature extraction. Therefore, incorporating temporal modeling is essential for accurately capturing fault dynamics and improving localization performance.

At the module level, all models exhibit reduced performance, reflecting the inherent challenges of fine-grained fault localization. This degradation is primarily attributed to the similarity of fault signatures within the same string and the limited resolution of available measurements. These findings indicate that diagnostic accuracy depends not only on model architecture but also on sensing resolution and signal separability.

Although the proposed CNN–LSTM framework achieved excellent fault diagnosis performance, some limitations should be acknowledged. First, the model was developed, trained, and validated using the same data collected from a single 5-kWp rooftop PV system under controlled experimental conditions. Consequently, the proposed framework may have limited generalizability to PV systems with different capacities. In addition, the current study considers only three representative fault types (open-circuit, short-circuit, and ground faults), whereas practical PV systems may experience more complex conditions, such as partial shading, module degradation, and hotspot formation.

5. Conclusion and Future Works

This research developed and implemented a comprehensive deep learning framework for the intelligent detection, classification, and multi-level localization of faults in rooftop photovoltaic systems. The study introduced a hybrid CNN–LSTM architecture that integrates the spatial feature extraction capabilities of one-dimensional convolutional neural networks with the sequential learning strengths of long short-term memory units. To validate the approach, a full-scale experimental rooftop PV prototype was constructed, enabling the collection of multivariate time-series data under various real-world fault

scenarios, including string-to-string, string-to-ground, and open-circuit conditions. The framework was systematically evaluated against standalone 1D-CNN and LSTM models to establish its effectiveness. Based on the experimental results and analysis, the following conclusions are drawn:

(1) The hybrid CNN-LSTM model consistently outperforms standalone 1D-CNN and LSTM architectures across all evaluation criteria, including accuracy, precision, recall, and F1-score.
(2) The proposed framework achieves exceptional performance levels, reaching 99.96% accuracy for fault type classification, 98.76% for string-level localization, and 99.21% for module-level localization.
(3) While 1D-CNNs are effective at capturing local signal patterns, modeling long-term temporal dependencies through LSTM units is essential for accurately capturing the time-varying fluctuations and evolving patterns inherent in PV fault dynamics.
(4) The system demonstrates high diagnostic robustness using a minimal set of commonly available signals - specifically string voltages, currents, and ambient temperature - making it a cost-effective and scalable solution for real-time monitoring in existing photovoltaic installations.

Future work will focus on collecting long-term field data under diverse environmental and operating conditions such as partial shading, module degradation, and hotspot formation, extending the framework to PV systems with different capacities, and validating real-time fault diagnosis on previously unseen PV systems.

Conflicts of Interest

The authors declare no conflict of interest.

Acknowledgements

This research was funded by Ho Chi Minh City University of Technology and Engineering, Vietnam, under grant No. 2026-148.

References

[1] S. Habib, M.Tamoor, M. M. Gulzar, P. ZakaUllah, A. F. Murtaza, and T. Alharbi, “Modeling and Integration of Rooftop Photovoltaic Systems for Sustainable Energy Access in Public Sector Buildings in Diverse Climates”, Scientific Reports, vol.15, no. 1, 2025.
[2] A. Hamza, Z. Ali, S. Dudley, K. Saleem, M. Uneeb, N. Christofides, “A Multi-stage Review Framework for AI-driven Predictive Maintenance and Fault Diagnosis in Photovoltaic Systems,” Applied Energy, vol. 393, article no. 126108, 2025.
[3] Y. Liu and Y. Wu, “Fault Diagnosis of Photovoltaic Modules: A Review,” Solar Energy, vol. 293, no. 1, article no. 113489, 2025.
[4] M. N. Abuhashish, A. Refaat, A. Kalas, M. S. Hamad, and M. H. Elfar, “Towards Accurate and Reliable Fault Diagnosis in PV Systems: Techniques, Challenges, and Future Directions,” Process Safety and Environmental Protection, vol. 198, article no. 107217, 2025.
[5] M. M. Rahman and A. K. Srivastava, “Detection, Classification, and Localization of Faults and Failures in Photovoltaic Arrays,” Discover Energy, vol. 6, article no. 26, 2026.
[6] R. V. Vichare and S. R. Gaikwad, “AI-based Predictive Maintenance of Solar Photovoltaics Systems: A Comprehensive Review,” Energy Informatics, vol. 8, no. 1, article no. 128, 2025.
[7] B. Aljafari, P. R. Satpathy, S. B. Thanikanti, and N. Nwulu, “Supervised Classification and Fault Detection in Grid-Connected PV Systems Using 1D-CNN: Simulation and Real-Time Validation,” Energy Reports, vol. 12, pp. 2156-2178, 2024.
[8] A. Seghiour, Y. Bendjeddou, I. M. Mostefaoui, A. Chouder, H. Alharbi, A. S. B. Humayd, et al., “Fault Detection and Diagnosis in Photovoltaic Systems Using Artificial Intelligence and Time-Frequency Analysis,” Scientific Reports, vol. 16, article no. 10056, 2026.

[9] S. R. Mohanty, M. U. Maruf, V. Singh, and Z. Ahmad, "Machine Learning Approaches for Automatic Defect Detection in Photovoltaic Systems," Solar Energy, vol. 198, article no. 113672, 2025.

[10] F. Kibrete, D. E. Woldemichael, and H. S. Gebremedhen, "Fault Diagnosis of Rotating Machines Based on Combination of One-Dimensional Convolutional Neural Network and Long Short-Term Memory in Variable Working Conditions", The Journal of Engineering, vol. 2025, no. 1, article no. 1670810, 2025.

[11] A. Mellit and S. Kalogirou, "Assessment of Machine Learning and Ensemble Methods for Fault Diagnosis of Photovoltaic Systems," Renewable Energy, vol. 184, pp. 1074-1090, 2022.

[12] M. Alrifaey, W. H. Lim, C. K. Ang, E. Natarajan, M. I. Solihin, M. R. M. Juhari, et al., "Hybrid Deep Learning Model for Fault Detection and Classification of Grid-Connected Photovoltaic System," IEEE Access, vol. 10, pp. 13852-13869, 2022.

[13] T. Huang, Q. Zhang, X. Tang, S. Zhao, and X. Lu, "A Novel Fault Diagnosis Method Based on CNN and LSTM and Its Application in Fault Diagnosis for Complex Systems," Artificial Intelligence Review, vol. 55, no. 2, pp. 1289-1315, 2022.

[14] Ö. Küçükalİ, M. H. Bozkurt, E. Ulutaş, and I. Bozkurt, "S2LU: An Activation Function Based on Skew Student's t-distribution for Improved Neural Network Performance," Neural Computing and Applications, vol.38, article no. 43, 2026

[15] C. Y. Hsu and W. C. Liu, "Multiple Time-Series Convolutional Neural Network for Fault Detection and Diagnosis and Empirical Study in Semiconductor Manufacturing," Journal of Intelligent Manufacturing, v.32, pp. 823-836, 2021.

[16] Y. Luo, X. Zheng, and B. Yang, "Photovoltaic Array Fault Diagnosis and Dynamic Reconfiguration Based on Improved YOLOv7 and QAGO," Discover Computing, vol. 29, article no. 146, 2026.

[17] B. Chu, J. Shu, C. Zhao, Y. Wang, H. Ning, X. Yan, et al., "A Hybrid TimeGAN–xLSTM–Transformer Framework for Photovoltaic Power Forecasting under Complex Environmental Conditions," Scientific Reports, vol. 16, article no. 8782, 2026.

[18] S. Bani, S. Afonaa-Mensah, A. Yahya, and D. Simango, "Data-driven Modeling of Solar Power Output Using a CNN–LSTM Approach," Sustainable Energy Research, vol. 13, no. 1, article no. 16, 2026.



Copyright© by the authors. Licensee TAETI, Taiwan. This article is an open access article distributed under the terms and conditions of the Creative Commons Attribution (CC BY-NC) license (https://creativecommons.org/licenses/by-nc/4.0/).